Journal of Alloys and Compounds 509 (2011) 5848–5852

Contents lists available at ScienceDirect

Journal of Alloys and Compounds

journal homepage: www.elsevier.com/locate/jallcom

Sensitized high-order ultraviolet upconversion emissions of Gd^{3+} by Er^{3+} in $NaYF_4$ microcrystals

Kezhi Zheng, Dan Zhao, Daisheng Zhang, Ning Liu, Feng Shi, Weiping Qin*

State Key Laboratory on Integrated Optoelectronics, College of Electronic Science and Engineering, Jilin University, 2699 Qianjin Street, Changchun 130012, China

ARTICLE INFO

Article history:
Received 30 September 2010
Received in revised form 23 February 2011
Accepted 24 February 2011
Available online 3 March 2011

Keywords:
High-order
Ultraviolet
Upconversion luminescence

ABSTRACT

High-order ultraviolet (UV) upconversion (UC) emissions of Gd^{3+} and Er^{3+} ions were observed in $NaYF_4$:Yb^{3+}/Gd^{3+}/Er^{3+} microcrystals under 980 nm excitation. These UC emissions came from six- and five-photon UC processes at low pump power range, which were confirmed by the pumping power dependences of UC fluorescence intensities. In these high-order UC processes, energy transfer (ET) processes of $Er^{3+} \rightarrow Gd^{3+}$ played crucial roles in populating the excited states of Gd^{3+} ions. Experiments on concentration variation and dynamic analysis revealed the ET processes between Er^{3+} and Gd^{3+} in detail. Some of possible population routes for populating excited Gd^{3+} ions were proposed based on spectral and dynamic analysis.

1. Introduction

In recent years, short-wavelength compact solid-state lasers have attracted much attention due to their wide range of applications including high density optical data storage, IR sensors, color displays, undersea communications, and so on [1–4]. As one of the available approaches for achieving the short-wavelength laser radiation, frequency UC based on certain rare-earth ions (RE^{3+}) in different matrix have been investigated widely in the past two decades. However, most studies about UC emissions of RE^{3+} ions have focused on the visible region, and only a few groups reported strong UV UC emissions [5–10]. Consequently, synthesizing the intense UV luminescent materials and investigating UV UC emission mechanism are the most important tasks for researchers to develop UV UC solid-state lasers.

Er^{3+} ions have a rich level structure with quasi-ladder long-lived excited states, which are favorable to act as both sensitizer and activator for frequency UC. Most researchers have used Er^{3+} as an activator in their previous studies, and only a few considered it as a sensitizer [11–16]. In addition, unlike Er^{3+}, Tm^{3+}, and Ho^{3+} ions, UC emissions based on Gd^{3+} ions have rarely been reported. As far as we know, there were only four papers reported by Gharavi and McPherson, Cao et al., Qin et al., and Chen et al. concerning the UC emissions of Gd^{3+} ions [13,17–19]. The first author found 281 and 313 nm UC emissions from ^6I_J and ^6P_J levels of Gd^{3+}, respectively. They used Er^{3+} ions as sensitizers and green lasers (522 and 546 nm) as pumping sources. Qin et al. used Yb^{3+} and Tm^{3+} ions as double sensitizers and excited the sample with a 980 nm continuous wave (CW) diode laser. In their experiments, high-order UC emissions of Gd^{3+} and Tm^{3+} ions have been detected. The last author used $NaGdF_4$ as the host material and found the near vacuum UV luminescence of Gd^{3+} and Er^{3+} ions under 974 nm excitation and assigned these UV UC emissions to the unusual super saturation UC processes. However, the ET routes between Er^{3+} and Gd^{3+} ions have not been analyzed well in their work. Consequently, further studies are still necessary to make clear the ET processes between Er^{3+} and Gd^{3+}, because it is benefit for understanding the complex UC mechanism and the unusual UC population behaviors at high-energy levels of Er^{3+} and Gd^{3+} in the codoped system. In addition, we surmised that β-$NaYF_4$, with a high refractive index and low phonon energy, would improve the high-order UC emissions of Gd^{3+} ions greatly.

In this work, we chose β-$NaYF_4$ as the host material and presented an observation of high-order UV UC emissions from Gd^{3+} and Er^{3+} ions in Yb^{3+}–Gd^{3+}–Er^{3+} codoped microcrystals under 980 nm excitation. In the $NaYF_4$:Yb^{3+}/Gd^{3+}/Er^{3+} system, both Yb^{3+} and Er^{3+} served as sensitizers in exciting Gd^{3+} ions. Under 980 nm excitation, Yb^{3+} ions absorbed infrared (IR) photons and transferred the energy to Er^{3+} ions successively. Further ET occurred from Er^{3+} to Gd^{3+} ions at high-energy excited states, and then resulted in the high-order UV UC emissions of Gd^{3+} ions. The bridging function of Er^{3+}, the ET from Er^{3+} to Gd^{3+}, and their high-order UV UC emissions in the codoped system are discussed here in detail.

* Corresponding author. Tel.: +86 431 85168240 8325; fax: +86 431 85168240 8325.
E-mail address: wpqin@jlu.edu.cn (W. Qin).

0925-8388/$ – see front matter © 2011 Elsevier B.V. All rights reserved.
doi:10.1016/j.jallcom.2011.02.144

2. Experimental

2.1. Chemicals

Y_2O_3, Yb_2O_3, Gd_2O_3, and Er_2O_3 (all with purity >99.99%, Shanghai Shabo Chemical Technology Co., Ltd., China), EDTA, NaF, and HNO_3 (all with purity of A.R., Beijing Fine Chemical Company, China). All the chemicals were used as received without further purification. RE_2O_3 (RE = Y, Yb, Gd, and Er) were dissolved in dilute HNO_3 by heating to prepare the stock solution of $RE(NO_3)_3$.

2.2. Sample preparation

Microcrystals $NaYF_4$ were synthesized *via* the ethylene diamine tetraacetic acid (EDTA)-assisted hydrothermal method according to the procedure described in Ref. [20]. In a typical procedure for the preparation of $NaYF_4$ microcrystals, 10 mL $Y(NO_3)_3$ (0.5 M) was added into 20 mL of aqueous solution containing 5 mmol of EDTA and magnetically stirred for 1 h, forming a chelated RE–EDTA complex. Then 20 mL NaF solution was added to the above mixture according to the RE^{3+}:F^- ratio of 1:16. After thorough stirring, the mixture was transferred into two 50 mL Teflon-lined stainless steel autoclaves. The autoclaves were sealed and maintained in an oven at 160 °C for 18 h, and then cooled down slowly to room temperature. The resulting precipitates were separated by centrifugation, washed with deionized water and ethanol several times, and then dried in air at 60 °C for 20 h. To improve the crystallinity of the microcrystalline powder, the sample was annealed in an argon atmosphere at 400 °C for 1.5 h. To investigate the luminescence properties of RE^{3+} in the codoped $NaYF_4$ microcrystals, the Yb^{3+}–Er^{3+} and Yb^{3+}–Gd^{3+}–Er^{3+} doped $NaYF_4$ samples were prepared by introducing proper amount of $Yb(NO_3)_3$, $Gd(NO_3)_3$, and Er $(NO_3)_3$ solution instead of $Y(NO_3)_3$ to the solution as described above.

2.3. Characterization

The crystal structures were analyzed by a Rigaku RU-200b X-ray powder diffractometer (XRD) using a nickel-filtered Cu-Ka radiation (λ = 1.5406 Å). The size and morphology were investigated by scanning electron microscope (SEM, Hitachi TM-1000). UC luminescence spectra were recorded using a Hitachi F-4500 fluorescence spectrophotometer which equipped with a 980 nm CW diode laser and detected by R928 (Hamamatsu). The temporal property was studied by using a 953.6 nm Raman shifter laser (pumped by the second harmonic of a Nd:YAG pulsed laser, pulse width 10 ns, repetition rate 10 Hz) and a digital oscilloscope. All measurements were performed at room temperature.

3. Results and discussion

3.1. Structure, morphology, and UC luminescence of Yb^{3+}–Er^{3+} and Yb^{3+}–Gd^{3+}–Er^{3+} codoped $NaYF_4$ microcrystals

Fig. 1 shows X-ray powder diffractometer (XRD) pattern and corresponding morphology of the $NaY_{0.585}F_4$:$Yb_{0.2}Gd_{0.2}Er_{0.015}$ microcrystals. Fig. 1(a) reveals that the sample is hexagonal phase, which is in good agreement with the standard values for the bulk hexagonal β-$NaYF_4$ (JCPDS no.16-0334). No other impurity peaks can be detected from the XRD patterns, indicating that the microcrystals are single-phased and RE^{3+} have effectively incorporated into the $NaYF_4$ host lattice. The corresponding morphological analysis, as shown in Fig. 1(b), describes that the microcrystals are hexagonal prisms with uniform size distribution (diameters are 2–3 μm and lengths 5 μm on average). The crystal structure, size, and morphology of $NaY_{0.785}F_4$:$Yb_{0.2}Er_{0.015}$ microcrystals are the same as those of the above sample and they were not shown here for simplicity. Under 980 nm excitation (power density = 20 W/cm^2), the annealed $NaYF_4$:Yb^{3+}(20%)/Gd^{3+}(20%)/Er^{3+}(1.5%) (molar ratio) microcrystals emitted bright UC fluorescence, as shown in Fig. 2. In the range from 250 to 330 nm, several emission peaks are clearly observed, as shown in Fig. 2(a). The emission centered at 253.8 nm can be assigned to the transition from $^6D_{9/2}$ to $^8S_{7/2}$ of Gd^{3+} ions. Two emissions peaked in the region of 270–282 nm came from the $^6I_J \rightarrow {}^8S_{7/2}$ transitions of Gd^{3+}. Emissions peaked at 306 and 312 nm originated from the $^6P_{5/2} \rightarrow {}^8S_{7/2}$ and $^6P_{7/2} \rightarrow {}^8S_{7/2}$ transitions of Gd^{3+}, respectively. In addition, the emission centered at 317 nm is assigned to the $^2P_{3/2} \rightarrow {}^4I_{15/2}$ transition of Er^{3+}. In this work, we mainly pay attention to the UV UC emissions of Gd^{3+} and Er^{3+} ions,

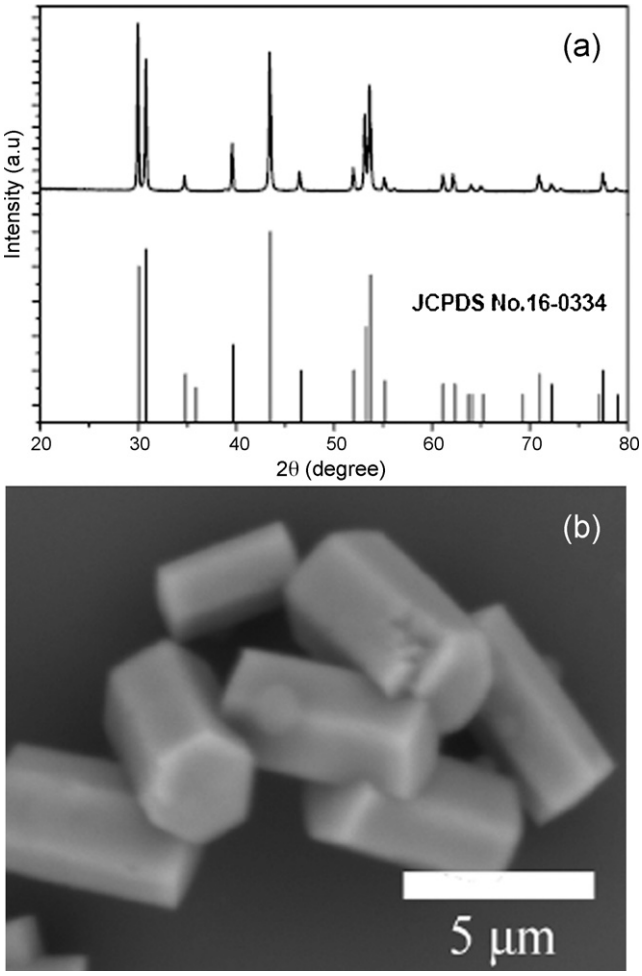

Fig. 1. XRD pattern and SEM image of $NaYF_4$:Yb^{3+}/Gd^{3+}/Er^{3+} microcrystals.

the well-known 350–750 nm UC emissions of Er^{3+}, as shown in Fig. 2(b), is described here briefly [21]. In the $NaYF_4$:Yb^{3+}/Gd^{3+}/Er^{3+} system, owing to the large energy gap between the ground state and the first excited state (32,000 cm^{-1}) of Gd^{3+} ions, Gd^{3+} cannot absorb 980 nm photons directly, therefore, there exist ET processes from Er^{3+} to Gd^{3+} at high energy excited states, which induced the

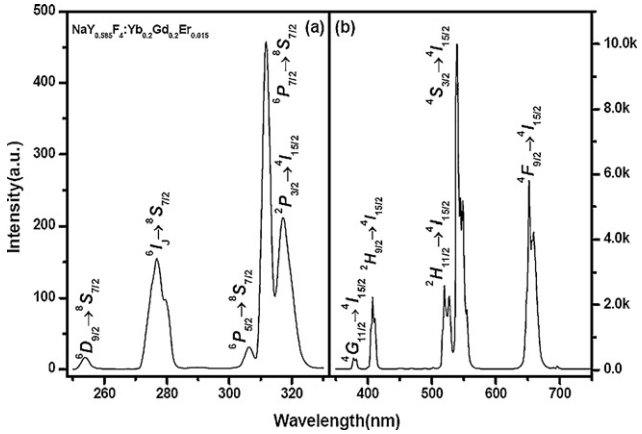

Fig. 2. UC luminescence spectra of $NaYF_4$:Yb^{3+}(20%)/Gd^{3+}(20%)/Er^{3+}(1.5%) (a) in the range of 250–330 nm; (b) in the range of 350–750 nm.

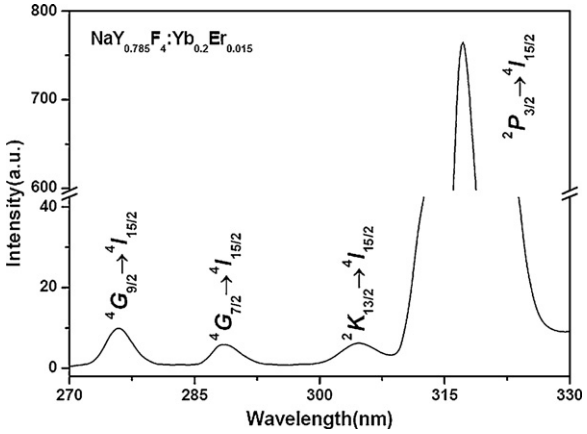

Fig. 3. UC luminescence spectrum of $NaYF_4$:Yb^{3+}(20%)/Er^{3+}(1.5%) in the range of 270–330 nm.

UC emissions of Gd^{3+} ions. Compared with the UC emission spectrum of $NaY_{0.785}F_4$:$Yb_{0.2}Er_{0.015}$ microcrystals, as shown in Fig. 3, we found that the weak emissions from $^4G_{9/2}$, $^4G_{7/2}$, and $^2K_{13/2}$ states of Er^{3+} (peaked at 276, 289, and 304 nm, respectively) vanished in the UC spectrum of $NaYF_4$:Yb^{3+}/Gd^{3+}/Er^{3+} microcrystals, as shown in Fig. 2(a). These can be attributed to two possible reasons as follows: the one is spectral overlap between Gd^{3+} and Er^{3+} ions (*e.g.* $^6I_J \rightarrow {}^8S_{7/2}$ *vs.* $^4G_{9/2} \rightarrow {}^4I_{15/2}$ and $^6P_{5/2} \rightarrow {}^8S_{7/2}$ *vs.* $^2K_{13/2} \rightarrow {}^4I_{15/2}$), and the other is ET from Er^{3+} to Gd^{3+}. In this codoped system, two routes are responsible for the depopulation of $^4G_{9/2}$, $^4G_{7/2}$, and $^2K_{13/2}$ states of Er^{3+}: (1) nonradiative relaxation (NR) to the lower level $^2P_{3/2}$; (2) ETs from the three states of Er^{3+} to the nearby Gd^{3+} ions to populate the excited states of Gd^{3+}. All these results could well explain why the weak emissions from Er^{3+} at high-energy states disappeared in the $NaY_{0.585}F_4$:$Yb_{0.2}Gd_{0.2}Er_{0.015}$ microcrystals. It is crucial important to clarify the bridging function of Er^{3+} ions and the ET processes between Gd^{3+} and Er^{3+} for understanding the complex UC mechanism and the possible population processes of high energy excited states of Gd^{3+} and Er^{3+} in this Yb^{3+}–Gd^{3+}–Er^{3+} tri-doped system, and these will be described below in detail.

3.2. Dynamic analysis and possible UC processes in the codoped system

Fig. 4 describes schematically possible upconverted processes in energy level diagrams of Yb^{3+}, Gd^{3+}, and Er^{3+} ions [22,23]. Under 980 nm excitation, Er^{3+} ions in the Yb^{3+}–Gd^{3+}–Er^{3+} tri-doped system accept the energy transferring from Yb^{3+} ions successively to populate the high-energy states $^4G_{9/2}$ by two different routes as following: $^4I_{15/2} \xrightarrow{ET} {}^4I_{11/2} \xrightarrow{ET} {}^4F_{7/2} \xrightarrow{NR} {}^2H_{11/2}$, $^4S_{3/2} \xrightarrow{ET} {}^2G_{7/2} \xrightarrow{NR} {}^4G_{11/2} \xrightarrow{ET} {}^4G_{9/2}$ (route 1); $^4I_{15/2} \xrightarrow{ET} {}^4I_{11/2} \xrightarrow{NR} {}^4I_{13/2} \xrightarrow{ET} {}^4F_{9/2} \xrightarrow{ET} {}^2H_{9/2} \xrightarrow{NR} {}^4H_{11/2}$, $^4S_{3/2} \xrightarrow{ET} {}^2G_{7/2} \xrightarrow{NR} {}^4G_{11/2} \xrightarrow{ET} {}^4G_{9/2}$ (route 2) [24]. Additionally, Er^{3+} at $^4G_{9/2}$ can relax nonradiatively to the $^4G_{7/2}$, $^2K_{13/2}$, and $^2P_{3/2}$ states, as depicted in Fig. 4. For the large energy gap between the ground state and the first excited state, the major mechanism in populating the excited states ^6I_J and ^6P_J of Gd^{3+} is the ET from Er^{3+} to Gd^{3+} ions. Combined with above analysis, three ET processes should be considered owing to their appropriate energy matching: $^4G_{9/2} \rightarrow {}^4I_{15/2}$ (Er^{3+}): $^8S_{7/2} \rightarrow {}^6I_J$ (Gd^{3+}) (ET1), $^4G_{7/2}$ and $^2K_{13/2} \rightarrow {}^4I_{15/2}$ (Er^{3+}):$^8S_{7/2} \rightarrow {}^6P_J$ (Gd^{3+}) (ET2 and 3, respectively). These ETs can be confirmed by the fluorescent dynamics of Er^{3+}, as shown in Fig. 5. The luminescence decay curves of Er^{3+} ions in both $NaYF_4$:Yb^{3+}(20%)/Gd^{3+}(20%)/Er^{3+}(1.5%) and $NaYF_4$:Yb^{3+}(20%)/Er^{3+}(1.5%) microcrystalline samples can be well fitted into single exponential function $I_{(t)} = I_0 \exp(-t/\tau)$, where I_0 is the initial emission intensity at $t = 0$, and τ is excited state lifetime. The lifetime τ for the $^4G_{9/2}$, $^4G_{7/2}$, $^2K_{13/2}$, and $^2P_{3/2}$ states of Er^{3+} in the two samples are labeled in the inset of Fig. 5. Obviously, the lifetimes of $^4G_{9/2}$, $^4G_{7/2}$, and $^2K_{13/2}$ states of Er^{3+} in $NaYF_4$:Yb^{3+}(20%)/Gd^{3+}(20%)/Er^{3+}(1.5%) shortened comparing to those of $NaYF_4$:Yb^{3+}(20%)/Er^{3+}(1.5%) microcrystals, while the lifetime of $^2P_{3/2}$ state almost keep unchanged for the two samples. By codoping Gd^{3+} ions into the $NaYF_4$:Yb^{3+}/Er^{3+} microcrystals, an extra route has been introduced to depopulate the Er^{3+} ions in the excited states and decrease their lifetimes due to the ETs to Gd^{3+} ions. In addition, owing to large energy mismatch (1200–2300 cm^{-1}) between $^2P_{3/2} \rightarrow {}^4I_{15/2}$ (Er^{3+}) and $^8S_{7/2} \rightarrow {}^6P_J$ (Gd^{3+}), which cannot be compensated by the phonon energy of $NaYF_4$ microcrystals, the ET between these two levels is ineffective, and thus the lifetime of $^2P_{3/2}$ state between two samples are almost the same. This result is in contradiction to

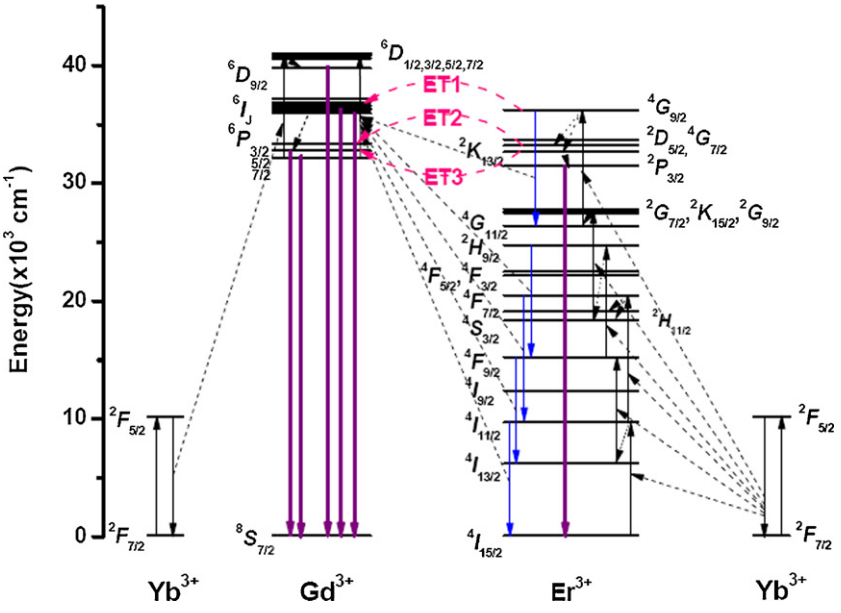

Fig. 4. Energy level diagrams of Yb^{3+}, Gd^{3+}, and Er^{3+} ions, and possible UC processes.

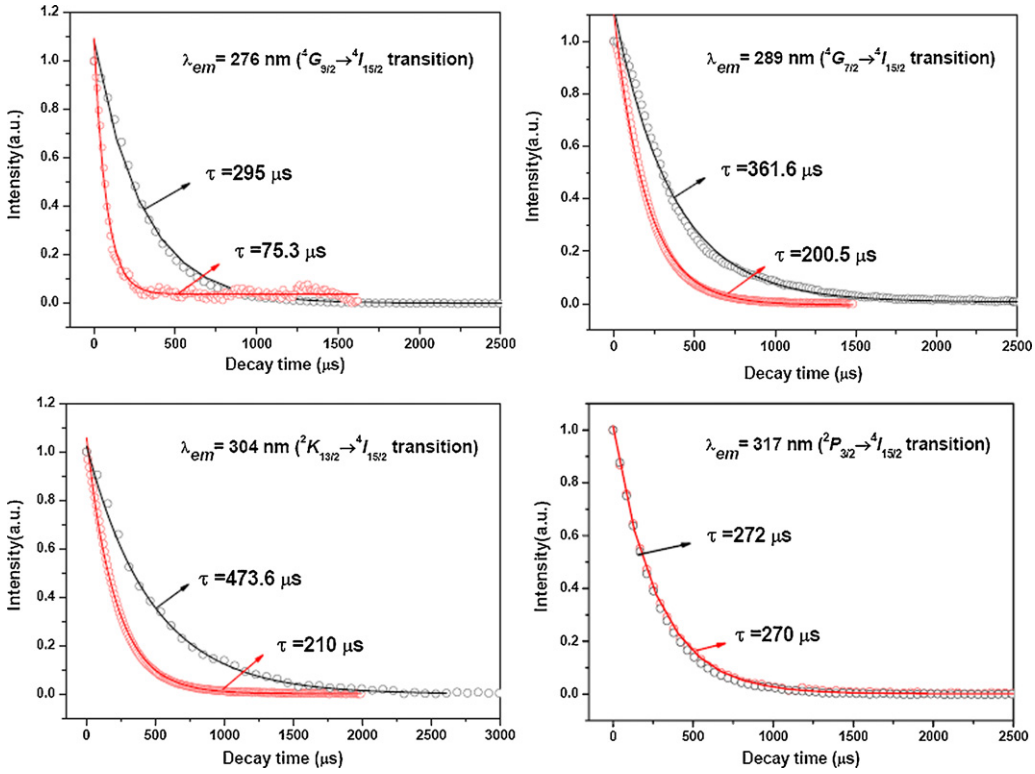

Fig. 5. The luminescence decay curves of Er^{3+} (λ_{ex} = 953.6 nm, λ_{em} = 276, 289, 304, and 317 nm; represent the $^4G_{9/2} \rightarrow {}^4I_{15/2}$, $^4G_{7/2} \rightarrow {}^4I_{15/2}$, $^2K_{13/2} \rightarrow {}^4I_{15/2}$, and $^2P_{3/2} \rightarrow {}^4I_{15/2}$ transitions, respectively) in $NaYF_4$:Yb^{3+}(20%)/Gd^{3+}(20%)/Er^{3+}(1.5%) (red circle) and $NaYF_4$:Yb^{3+}(20%)/Er^{3+}(1.5%) (black circle) microcrystals. Open circles: experimental data; solid lines: fitting results by $I_{(t)} = I_0 \exp(-t/\tau)$. The insets are lifetime τs for these two samples, respectively. (For interpretation of the references to color in this figure legend, the reader is referred to the web version of the article.)

the previous results reported on Yb^{3+}-Er^{3+} codoped $NaGdF_4$ sample [19]. At room temperature, the nonradiative relaxation probability of $^6I_J \rightarrow {}^6P_J$ is much larger than the radiative transition probability of $^6I_{7/2} \rightarrow {}^8S_{7/2}$, which provide another way to populate the ^6P_J levels [25]. For the UC emission from ^6D_J of Gd^{3+} in the $NaYF_4$:Yb^{3+}/Gd^{3+}/Er^{3+} microcrystals, as shown in Fig. 4, due to the appropriate energy matching, the transitions of $^2F_{5/2} \rightarrow {}^2F_{7/2}$ (~10,000 cm^{-1}), $^4I_{11/2} \rightarrow {}^4I_{15/2}$ (~9800 cm^{-1}), $^4F_{9/2} \rightarrow {}^4I_{13/2}$ (~9100 cm^{-1}), $^2H_{11/2} \rightarrow {}^4I_{11/2}$ (~9200 cm^{-1}), $^2H_{9/2} \rightarrow {}^4F_{9/2}$ (~9400 cm^{-1}), and $^4G_{9/2} \rightarrow {}^4G_{11/2}$ (~10,000 cm^{-1}) can offer approximate energy for the transition of $^6P_J \rightarrow {}^6D_J$ (~6500–8500 cm^{-1}). Owing to the strong IR absorption of Yb^{3+} and the high concentration of Yb^{3+} ions in the sample, $^2F_{5/2} \rightarrow {}^2F_{7/2}$ (Yb^{3+}): $^6P_J \rightarrow {}^6D_J$ (Gd^{3+}) should be the dominant approach in populating the ^6D_J level. Based on the above analysis, we deduced that it is of central importance to populate the $^4G_{9/2}$, $^4G_{7/2}$, and $^2K_{13/2}$ levels of Er^{3+} efficiently to obtain intense UV UC emissions of Gd^{3+} in the Yb^{3+}–Gd^{3+}–Er^{3+} codoped $NaYF_4$ microcrystals.

3.3. Concentration-dependent UV UC emissions of Gd^{3+} and Er^{3+}

Fig. 6 shows UC emission spectra of samples $NaY_{0.785-x}F_4$:$Yb_{0.2}Gd_xEr_{0.015}$ (x = 0.05, 0.1, 0.15, and 0.2) in the range of 250–330 nm, which were all recorded under the same conditions. It was found that with the increase of Gd^{3+} concentration, all the emissions from Gd^{3+} increased, while the emission intensity of Er^{3+} decreased. One of the most likely reasons for the intensity variation is that the incorporation of an elevated amount of Gd^{3+} dopants into the $NaYF_4$ host lattice would decrease the average interatomic distance between Er^{3+} and Gd^{3+} ions and thus facilitate the ETs between them efficiently. Therefore, by doping different concentrations of Er^{3+} and Gd^{3+} into $NaYF_4$ host lattice, we could control the population processes of their high energy excited states in the co-doped systems, and it is an effective way to investigate the ET processes between the RE^{3+} in the codoped system.

3.4. Power-dependent UV UC luminescence of Gd^{3+} and Er^{3+}

In order to understand the UC mechanism well, we investigated the pumping power dependence of UC fluorescence intensity. For an unsaturated UC process, the emission intensity I_f is proportional to the n-th power of the IR excitation intensity I_{IR}: $I_f \propto I_{IR}^n$, where n is the number of IR photons absorbed per upconverted photon emitted. [26] Fig. 7 shows the double logarithmic plots of I_f as a function of I_{IR}. The n values can be easily obtained from the slope of the linear fit. Obviously, for a certain emission, n varies from low to high pump

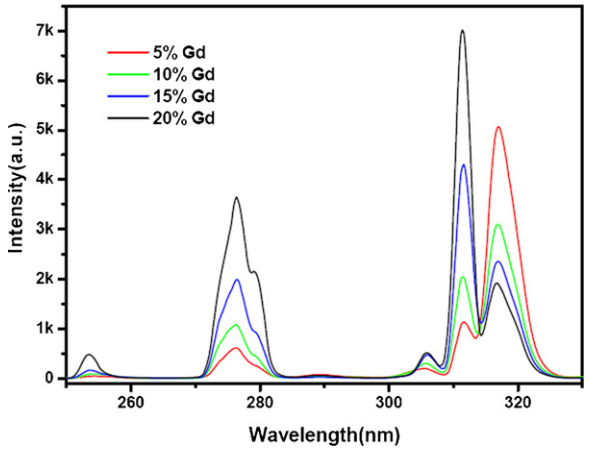

Fig. 6. UC emission spectra of annealed samples $NaY_{0.785-x}F_4$:$Yb_{0.2}Gd_xEr_{0.015}$ (x = 0.05, 0.1, 0.15, and 0.2) in the range of 250–330 nm.

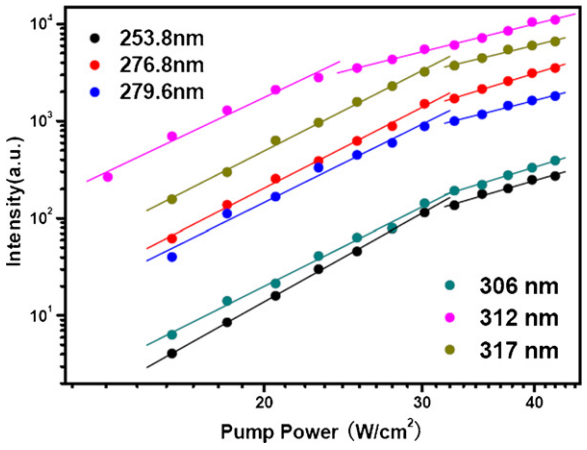

Fig. 7. Plots (log–log) of emission intensity versus excitation power in $NaYF_4$:Yb^{3+}/Gd^{3+}/Er^{3+} microcrystals.

Table 1
The calculated *ns* for the $NaYF_4$:Yb^{3+}/Gd^{3+}/Er^{3+} microcrystals under low and high power region, respectively.

Wavelength (nm)	Low energy region (10–30 W/cm²)	High energy region (30–50 W/cm²)
253.8	5.17 ± 0.0	2.68 ± 0.2
276.8	4.74 ± 0.0	2.83 ± 0.1
279.6	4.58 ± 0.0	2.3 ± 0.1
306	4.63 ± 0.0	2.8 ± 0.1
312	4.38 ± 0.0	2.3 ± 0.0
317	4.7 ± 0.1	2.24 ± 0.1

power regions. For the sample $NaY_{0.585}F_4$:$Yb_{0.2}Gd_{0.2}Er_{0.015}$ and in low pump power region, the slope *n* is 5.17 for the $^6D_{9/2} \rightarrow {}^8S_{7/2}$ transition of Gd^{3+}, which indicates that populating the $^6D_{9/2}$ level need six 980 nm photons and is a six-photon process. For the 276.8, 279.6, 306, and 312 nm UC emissions of Gd^{3+}, the *ns* we obtained are all lie between 4 and 5, indicating five-photon processes. Additionally, for the $^2P_{3/2} \rightarrow {}^4I_{15/2}$ transition of Er^{3+}, the calculated *n* is 4.7, describing a five-photon process. The obtained *ns* for these UV UC emissions are close to the actually numbers of 980 nm photon absorbed by Er^{3+} and Gd^{3+}, indicating these emissions came from unsaturated UC processes in the power range of 10–30 W/cm². On the other hand, when the pump power was increased to 30–50 W/cm², the calculated *ns* for all the emissions decrease greatly, as shown in Table 1, which could be attributed to the thermal effect resulting from the laser radiation.

4. Conclusions

In conclusion, Yb^{3+}/Gd^{3+}/Er^{3+} codoped $NaYF_4$ microcrystals were synthesized successfully through a facile EDTA-assisted hydrothermal method. After annealing, the microcrystals emitted UV UC fluorescence and presented the characteristic emissions of Gd^{3+} and Er^{3+} ions under 980 nm excitation. Power dependence analysis confirmed that these UC emissions came from five- and six-photon processes in low power region. In the complex frequency UC processes, ETs from Er^{3+} to Gd^{3+} play crucial roles in populating the excited Gd^{3+} and producing the high-order UV UC emissions of Gd^{3+}. Experiments on spectral and dynamic analysis demonstrated some of possible ET routes between Er^{3+} and Gd^{3+}. Additionally, the ET between $^2P_{3/2}$ of Er^{3+} and ^6P_J of Gd^{3+} was excluded in the codoped system by dynamical analysis as well.

Acknowledgment

This work was supported by the National High Technology Research and Development Program of China (863 Program: 2009AA03Z309) and the National Natural Science Foundation of China (NNSFC) (grants 10874058 and 60908031).

References

[1] T. Hebert, R. Wannemacher, W. Lenth, R. Macfarlane, Appl. Phys. Lett. 57 (1990) 1727–1729.
[2] Y. Mita, K. Hirama, N. Ando, H. Yamamoto, S. Shionoya, J. Appl. Phys. 74 (1993) 4703.
[3] S. Georgescu, O. Toma, Proc. SPIE 5581 (2004) 245.
[4] W. Shi, M. Bass, M. Birnbaum, J. Opt. Soc. Am. B 7 (1990) 1456–1462.
[5] F. Auzel, J. Lumin. 45 (1990) 341–345.
[6] C.J. da Silva, M.T. de Araujo, E.A. Gouveia, A.S. Gouveia-Neto, Appl. Phys. B-Lasers O 70 (2000) 185–188.
[7] G. Qin, W. Qin, C. Wu, S. Huang, J. Zhang, S. Lu, D. Zhao, H. Liu, J. Appl. Phys. 93 (2003) 4328.
[8] I.I. Leonidov, V.G. Zubkov, A.P. Tyutyunnik, N.V. Tarakina, L.L. Surat, O.V. Koryakova, E.G. Vovkotrub, J. Alloys Compd. 509 (2011) 1339–1346.
[9] P.V. dos Santos, E.A. Gouveia, M.T. de Araujo, A.S. Gouveia-Neto, A.S.B. Sombra, J.A. Medeiros Neto, Appl. Phys. Lett. 74 (1999) 3607.
[10] H. Du, W. Zhang, J. Sun, J. Alloys Compd. 509 (2011) 3413–3418.
[11] M. Hehlen, K. Kr mer, H. Güdel, R. McFarlane, R. Schwartz, Phys. Rev. B 49 (1994) 12475–12484.
[12] A. Amarnath Reddy, S. Surendra Babu, K. Pradeesh, C.J. Otton, G. Vijaya Prakash, J. Alloys Compd. 509 (2011) 4047–4052.
[13] A.R. Gharavi, G.L. McPherson, J. Opt. Soc. Am. B 11 (1994) 913–918.
[14] G. Qin, W. Qin, S. Huang, C. Wu, D. Zhao, B. Chen, S. Lu, E. Shulin, J. Appl. Phys. 92 (2002) 6936.
[15] A.S. Oliveira, M.T. de Araujo, A.S. Gouveia-Neto, A.S.B. Sombra, J.A. Medeiros Neto, J. Appl. Phys. 83 (1998) 604.
[16] A.S. Oliveira, M.T. de Araujo, A.S. Gouveia-Neto, J.A. Medeiros Neto, A.S.B. Sombra, Appl. Phys. Lett. 72 (1998) 753.
[17] C. Cao, W. Qin, J. Zhang, Y. Wang, P. Zhu, G. Wei, G. Wang, R. Kim, L. Wang, Opt. Lett. 33 (2008) 857–859.
[18] W. Qin, C. Cao, L. Wang, J. Zhang, D. Zhang, K. Zheng, Y. Wang, G. Wei, G. Wang, P. Zhu, Opt. Lett. 33 (2008) 2167–2169.
[19] G. Chen, H. Liang, H. Liu, G. Somesfalean, Z. Zhang, Opt. Express 17 (2009) 16366–16371.
[20] G. Wang, W. Qin, L. Wang, G. Wei, P. Zhu, R. Kim, Opt. Express 16 (2008) 11907–11914.
[21] A.S. Gouveia-Neto, E.B. da Costa, L.A. Bueno, S.J.L. Ribeiro, J. Alloys Compd. 375 (2004) 224.
[22] W.T. Carnall, P.R. Fields, K. Rajnak, J. Chem. Phys. 49 (1968) 4412–4424.
[23] W.T. Carnall, P.R. Fields, K. Rajnak, J. Chem. Phys. 49 (1968) 4424–4442.
[24] K. Zheng, L. Wang, D. Zhang, D. Zhao, W. Qin, Opt. Express 18 (2010) 2934–2939.
[25] J. Sytsma, G. Imbusch, G. Blasse, J. Phys.: Condens. Matter 2 (1990) 5171–5178.
[26] M. Pollnau, D.R. Gamelin, S.R. Lüthi, H.U. Güdel, M.P. Hehlen, Phys. Rev. B 61 (2000) 3337–3346.